Basrah Journal of Science Vol. 38 (2), 198-222, 2020

Simulation of Newtonian axisymmetric pipe flow by using a Taylor Galerkin/pressure correction finite element method

Ihssan A. Fadhel [1], Alaa H. Al-Muslimawi [2]

1. Department of Mathematics, College of Education for Pure Sciences, University of Basrah, Basra, Iraq
2. Department of Mathematics, College of Sciences, University of Basrah, Basra, Iraq

Corresponding authors: Ihssan A. Fadhel, e-mail: ihssanaqeel@yahoo.com
Alaa H. Al-Muslimawi, e-mail: alaa.abdullah@uobasrah.edu.iq

Doi 10.29072/basjs.202024

Article inf.

Received: 07/5/2020

Accepted 15/7/2020

Published 31/8/2020

Keywords:

Finite element methods; Galerkin method; Naiver-Stoke equations; Newtonian fluid; Taylor expansion.

Abstract

In this study, a time stepping Taylor Galerkin/pressure correction finite element scheme $(TS-TG/PC-FEM)$ is employed to treat incompressible Newtonian flows. In this context, Navier-Stoke partial differential equations have been used to describe the motion of the fluid. The equations consist of a time-dependent continuity equation for conservation of mass and time-dependent conservation of momentum equations. Examples considered include a start-up of Poiseuille, flow in a axisymmetric rectangular channel for the Newtonian fluid. This test is conducted by taking a circular section of the pipe. The critical level of Re number is investigated under the effect of various parameters. Moreover, the effect of viscosity variation and the boundary maximum axial velocity $((u_z)_{max})$ that imposed at the inlet upon the solution is studied as well. In this manner, the findings reveal that, there is a significant effect from viscosity variation and $((u_z)_{max})$ value on the level of Re number such that the extremely limit of Re number that can be reached was around 576 with $(u_z)_{max}=1$ and $\mu=1$. In contrast, the results shown that the influence of viscosity variation was an opposite of what that was in the case of Re number situation, where the high viscosity gave high level of density. The influence of geometry design on the level of pressure drop and pressure coefficient is covered in this article.

1. Introduction

The solution of the system of differential equations governing the flow of Newtonian fluids, has attached some considerable attention in the field of computational fluid dynamics (CFD). For a simple shear flow, under constant pressure and temperature, Newtonian fluids exhibit a linear relationship between shear stress and shear rate through a constant viscosity. The behaviour of such fluids can be predicted on the basis of the Navier-Stokes differential equations. This system is presented by the mass conservation and momentum partial differential equations (see for example Bird et al.[1] for details). Numerically, a time stepping Taylor-Galerkin/pressure correction method $(TS-TG/PC-FEM)$ is implemented in current study. This approach is introduced by Townsend and Webster [2] to treat viscous incompressible flows of Newtonian and non-Newtonian fluids. The main difference of this method from other earlier mixed methods is that the velocity and pressure variables are disassembled. Basically, the separation idea of the problem variables is inspired from the investigation of Chorin [3]. Over the previous time, two essential trends have taken to treat such governing equations. First way has known as the fractional step method, which is favored by Gresho et. al. [4] and Donea et. al.[5]. In contrast, there is another trend that be used to solve the governing equations of flow based on the velocity correction approach (see Kawahara and Ohmiya [6]). The significant difference between the two methods is that for the former the separation of velocity and pressure is effected after the GFEM discretization of the differential equations, while for the final, it happens at the differential equation stage.

On the other hand, the most suitable numerical technique within the finite element framework for solution of the differential equations is a time stepping Taylor Galerkin pressure correction $(TGPC)$ finite element scheme (for more details see Al-Muslimawi [7]). This approach involves two methods, a Taylor Galerkin method and a pressure correction method. The Taylor Galerkin method is a two-step Lax-Wendroff time stepping procedure (predictor-corrector), extracted via a Taylor series expansion in time (Donea [8], Zinenkiewicz et al. [9]). The pressure-correction method accommodates the incompressibility constraint to ensure second-order accuracy in time (see Hawken et al. [10], Aboubacar et al. [11]). Amazing attentions spent to treat the flow problems in the cartesian coordinates by using

$TS-TG/PC-FEM$ (see for example [7], [10], [12], [13]). In contrast, for treating the axisymmetric problems using this scheme is not easy, such that the studies around the such problems were limitted. Thus, we spent more a concentration on this type of interesting investigation. In this study, a $(\mathrm{TS-TG/PC-FEM})$ is employed to solve sets of differential equations. The novelty here is to study the effect of viscosity variation and the boundary maximum axial velocity $((\mathrm{u_z})_{\mathrm{max}})$ on the system solution that is taken to be steady state, incompressible, axisymmetric, and laminar, which has not been addressed by researchers previously. In this context, Poiseuille (Ps) flow along a two-dimensional planar straight channel under isothermal conditions is studied. The main results of the current study focused on determining the critical levels of Reynolds number (Re), which also reoresents the excited issue of this study. Moreover, the geometry design reflected a significant effect on the level of pressure drop and pressure coefficient.

2. Mathematical Modeling

The governing equations for incompressible Newtonian liquid, which consist of momentum and continuity equations in the absence of body forces, can be stated as:

$$\nabla \cdot u = 0, \tag{1}$$

$$\rho \frac{\partial u}{\partial t} + \rho u \cdot \nabla u = \nabla \cdot T - \nabla p, \tag{2}$$

where, u, p and ρ are the velocity, pressure and density of fluid, respectively. Here, the extra stress tensor T is defined as

$$T = 2\mu d. \tag{3}$$

Correspondingly, the rate of deformation d for general flows is expressed as,

$$d = \frac{1}{2}(\nabla u + \nabla u^{\dagger}), \tag{4}$$

where $\dagger$ is the tensor transpose. In addition, the momentum equation (2) can also be expressed in the non-dimensional form as

$$Re \frac{\partial u}{\partial t} + Re\, u \cdot \nabla u = \nabla \cdot (2\beta d) - \nabla p. \tag{5}$$

Here, $Re = \rho \frac{UL}{\mu}$ is a Reynolds number, which is defined based on velocity (U), length (L) and density (ρ). Moreover, (β) is provided as the viscosity of fluid (for more details see [14]-[17]).

Our study aims to introduce a study in incompressible lamnar axisymmetric flow; thus, the system of non-dimensional differential equations for incompressible flow with absent forces can be expressed in cylindrical coordinates as:

Continuity equation

$$\frac{\partial u_r}{\partial r} + \frac{1}{r} u_r + \frac{1}{r} \frac{\partial u_\theta}{\partial \theta} + \frac{\partial u_z}{\partial z} = 0. \tag{6}$$

Momentum equation

$$\frac{\partial u_r}{\partial t} + (\bar{u} \cdot \nabla) u_r = -\frac{1}{Re} \frac{\partial p}{\partial r} + \frac{\beta}{Re} (\nabla^2 u_r), \tag{7}$$

$$\frac{\partial u_\theta}{\partial t} + (\bar{u} \cdot \nabla) u_\theta = -\frac{1}{Re} \frac{\partial p}{\partial \theta} + \frac{\beta}{Re} (\nabla^2 u_\theta), \tag{8}$$

$$\frac{\partial u_z}{\partial t} + (\bar{u} \cdot \nabla) u_z = -\frac{1}{Re} \frac{\partial p}{\partial z} + \frac{\beta}{Re} (\nabla^2 u_z). \tag{9}$$

Where, u_r, u_θ and u_z are the velocity components in r-direction, θ-direction and z-direction, respectively.

3. Numerical method

In this study a $TS - TG/PC - FEM$ is utilized to treat the system of current differential equations. In this situation, the two-step Lax-Wendroff method is used to achieve second-order accuracy in both time and space. To explain the derivative of such method, consider a one-dimensional problem of the form:

$$\frac{\partial u}{\partial t} = G(u), \tag{10}$$

and using

$$\frac{\partial^2 u}{\partial t^2} = \frac{\partial G}{\partial t} = \frac{\partial G}{\partial u} \frac{\partial u}{\partial t} = \frac{\partial G}{\partial u} G, \tag{11}$$

a second-order Taylor expansion of u around t^n results in the following expression

$$u^{n+1} = u^n + \Delta t\left(\frac{\partial u}{\partial t}\right)^n + \frac{1}{2}(\Delta t)^2\left(\frac{\partial^2 u}{\partial t^2}\right)^n,$$

$$u^{n+1} = u^n + \Delta t G^n + \frac{1}{2}(\Delta t)^2\left(\frac{\partial G}{\partial u}\right)^n G^n, \quad (12)$$

where, the superscript n denotes the time level. To obviate the explicit evaluation of the first derivative $\frac{\partial G}{\partial u}$, a two-step Lax-Wendroff scheme is utilized to gain an $O(\Delta t^2)$.

Therefore, the two-step Lax-Wendroff procedure over split time-step $t \in [t^n, t^{n+\frac{1}{2}}]$ and $t \in [t^n, t^{n+1}]$ is

$$step1: u^{n+\frac{1}{2}} = u^n + \frac{\Delta t}{2} G^n, \quad (13a)$$

$$step2: u^{n+1} = u^n + \Delta t G^{n+\frac{1}{2}}. \quad (13b)$$

In these equations, terms with n indicate evaluation at a specific time step.

For non-dimensional incompressible Newtonian fluid equation (5) is written as:

$$\frac{\partial u}{\partial t} = \frac{1}{Re}[L(u,d) - \nabla p], \quad (14)$$

where $L(u,d) = \nabla \cdot (2\beta d) - Re\ u \cdot \nabla u$. Then the fractional-staged formulations with non-dimensional parameters within each time-step may be given by:

$$stage1a: \frac{2Re}{\Delta t}\left[u^{n+\frac{1}{2}} - u^n\right] = L(u^n, d^n) - \nabla p^n, \quad (15a)$$

$$stage1b: \frac{Re}{\Delta t}[u^* - u^n] = L\left(u^{n+\frac{1}{2}}, d^{n+\frac{1}{2}}\right) - \nabla p^n, \quad (15b)$$

$$stage2: \nabla^2(p^{n+1} - p^n) = \frac{Re}{\theta \Delta t}\nabla \cdot u^*, \quad (15c)$$

$$stage\ 3: u^{n+1} - u^* = -\frac{\theta \Delta t}{Re}[\nabla(p^{n+1} - p^n)]. \quad (15d)$$

The summary of this method, the algorithm consists of three stages over each time $[t_n, t_{n+1}]$; in the first stage contain two sub-stages. In the start , at $stage\ 1a$, can computed a velocity component at half time step $(n + \frac{1}{2})$ by using the data raised at time n. At $stage\ 1b$, a velocity component u^* is computed from data that is found in stage 1a. At $stage\ 2$, the pressure difference over the time step is determined depending on the value of u^*, which is evaluated from step 1b. Finally, the value velocity time $n + 1$ are calculated by using U^*, and pressure difference $(p^{n+1} - p^n)$.

For the finite element method, we introduce approximations $u(x,t)$ and $p(x,t)$ to the velocity and pressure respectively over finite dimensional function spaces. Hence we get;

$$u(x,t) = \sum_{j=1}^{J_u} u_j(t)\phi_j(x),$$
$$p(x,t) = \sum_{j=1}^{J_p} p_j(t)\psi_j(x). \tag{16}$$

Such that J_u and J_p are the total number of nodes and the number of vertices only of the triangles, respectively. Here, $u_j(t)$ and $p_j(t)$ represent the vector of nodal values of velocity and pressure and $\phi_j(x), \psi_j(x)$ are their respective basis (shape or interpolation) functions. Similar forms apply for u^* and pressure difference. The domain Ω is partitioned into triangular elements with velocities computed at the vertex and mid side nodes, and pressure only at vertex nodes. For the shape functions, $\phi_j(x)$ are selected as quadratic basis functions and $\psi_j(x)$ as linear basis functions. The corresponding a $TS-TG/PC-FEM$ form of equations ((15a), (15b), (15c) and (15d)) may then be written in matrix form as (see [10]):

$$stepe\ 1a: \left[\frac{2Re}{\Delta t}M + \frac{1}{2}S\right]\left(U^{n+\frac{1}{2}} - U^n\right) = \{-[S + Re\ N(U)]U + \ell^{\dagger}\ P\}^n, \tag{17a}$$

$$stepe\ 1b: \left[\frac{Re}{\Delta t}M + \frac{1}{2}S\right](U^* - U^n) = \{-SU + \ell^{\dagger}\ P\}^n - Re[N(U)U]^{n+\frac{1}{2}}, \tag{17b}$$

$$stepe\ 2: K(P^{n+1} - P^n) = -\frac{Re}{\theta\Delta t}\ell U^*, \tag{17c}$$

$$stepe\ 3: \frac{Re}{\Delta t}M(U^{n+1} - U^*) = \theta\ell^{\dagger}(P^{n+1} - P^n). \tag{17d}$$

Consequently, the above matrices in an (r,θ,z) −coordinate system are defined as:

1. Mass Matrix,

$$M = \begin{bmatrix} M^{rr} & 0 & 0 \\ 0 & M^{\theta\theta} & 0 \\ 0 & 0 & M^{zz} \end{bmatrix}, \tag{18}$$

such that,

$$M^{rr} = M^{\theta\theta} = M^{zz} = \int_{\Omega^e} \phi\phi^{\dagger}\, d\Omega. \tag{19}$$

2. Convective Matrix,

$$N = \begin{bmatrix} C & D_1 & 0 \\ D_2 & C & 0 \\ 0 & 0 & C \end{bmatrix}, \tag{20}$$

where,

$$[C(u_r, u_\theta, u_z)] = \int_{\Omega^e} \left(\phi\phi^\dagger u_r \frac{\partial \phi^\dagger}{\partial r} + \frac{1}{r}\phi\phi^\dagger u_\theta \frac{\partial \phi^\dagger}{\partial \theta} + \phi\phi^\dagger u_z \frac{\partial \phi^\dagger}{\partial z} \right) d\Omega. \tag{21}$$

$$[D_1(u_\theta)] = -\int_{\Omega^e} \frac{1}{r}\phi\phi^\dagger u_\theta \phi^\dagger d\Omega, [D_2(u_\theta)] = \int_{\Omega^e} \frac{1}{r}\phi\phi^\dagger u_\theta \phi^\dagger d\Omega. \tag{22}$$

3. Momentum Diffusion Matrix,

$$S = \begin{bmatrix} S^{rr} & S^{r\theta} & S^{rz} \\ S^{\theta r} & S^{\theta\theta} & S^{\theta z} \\ S^{zr} & S^{z\theta} & S^{zz} \end{bmatrix}, \tag{23}$$

where,

$$S^{rr} = \int_{\Omega^e} \left(2\frac{\partial \phi}{\partial r}\frac{\partial \phi^\dagger}{\partial r} + \frac{1}{r^2}\frac{\partial \phi}{\partial \theta}\frac{\partial \phi^\dagger}{\partial \theta} + \frac{2}{r^2}\phi\phi^\dagger + \frac{\partial \phi}{\partial z}\frac{\partial \phi^\dagger}{\partial z} \right) d\Omega.$$

$$S^{r\theta} = (S^{\theta r})^\dagger = \int_{\Omega^e} \left(\frac{2}{r^2}\phi\frac{\partial \phi^\dagger}{\partial \theta} - \frac{1}{r^2}\frac{\partial \phi}{\partial \theta}\phi^\dagger + \frac{1}{r}\frac{\partial \phi}{\partial \theta}\frac{\partial \phi^\dagger}{\partial r} \right) d\Omega,$$

$$S^{rz} = \int_{\Omega^e} \left[\frac{\partial \phi}{\partial r}\frac{\partial \phi^\dagger}{\partial z} \right] d\Omega,$$

$$S^{\theta\theta} = \int_{\Omega^e} \left(\frac{\partial \phi}{\partial r}\frac{\partial \phi^\dagger}{\partial r} - \frac{1}{r}\frac{\partial \phi}{\partial r}\phi^\dagger + \frac{2}{r^2}\frac{\partial \phi}{\partial \theta}\frac{\partial \phi^\dagger}{\partial \theta} + \frac{2}{r^2}\phi\phi^\dagger - \frac{1}{r}\phi\frac{\partial \phi^\dagger}{\partial r} + \frac{\partial \phi}{\partial z}\frac{\partial \phi^\dagger}{\partial z} \right) d\Omega,$$

$$S^{\theta z} = (S^{z\theta})^\dagger = \int_{\Omega^e} \left[\frac{1}{r}\frac{\partial \phi}{\partial z}\frac{\partial \phi^\dagger}{\partial \theta} \right] d\Omega,$$

$$S^{zr} = \int_{\Omega^e} \left[\frac{\partial \phi}{\partial z}\frac{\partial \phi^\dagger}{\partial r} \right] d\Omega,$$

$$S^{zz} = \int_{\Omega^e} \left[\frac{\partial \phi}{\partial r}\frac{\partial \phi^\dagger}{\partial r} + \frac{1}{r^2}\frac{\partial \phi}{\partial \theta}\frac{\partial \phi^\dagger}{\partial \theta} + 2\frac{\partial \phi}{\partial z}\frac{\partial \phi^\dagger}{\partial z} \right] d\Omega.$$

4. divergence/pressure gradient matrix,

$$\ell = [\ell_r, \ell_\theta, \ell_z,]$$

$$\ell_r = \int_{\Omega^e} \left[\psi\frac{\partial \phi^\dagger}{\partial r} + \frac{1}{r}\psi\phi^\dagger \right] d\Omega, \ell_\theta = \int_{\Omega^e} \psi\frac{\partial \phi^\dagger}{\partial \theta} d\Omega, \ell_z = \int_{\Omega^e} \psi\frac{\partial \phi^\dagger}{\partial z} d\Omega.$$

5. A pressure stiffness matrix

$$K = \int_{\Omega^e} \left[\frac{\partial \psi}{\partial r} \frac{\partial \psi^\dagger}{\partial r} + \frac{\partial \psi}{\partial z} \frac{\partial \psi^\dagger}{\partial z} \right] d\Omega. \tag{24}$$

Furthermore, quadratic shape functions of the velocity components in cylindrical coordinates are used. These functions are given in the usual coordinates as:

$$\begin{bmatrix} \phi_1 \\ \phi_2 \\ \phi_3 \\ \phi_4 \\ \phi_5 \\ \phi_6 \end{bmatrix} = \begin{bmatrix} L_1^2 - L_1(L_2 + L_3) \\ L_2^2 - L_2(L_3 + L_1) \\ L_3^2 - L_3(L_1 + L_2) \\ 4L_1L_2 \\ 4L_2L_3 \\ 4L_3L_1 \end{bmatrix} = \begin{bmatrix} 1 & 0 & 0 & -1 & 0 & -1 \\ 0 & 1 & 0 & -1 & -1 & 0 \\ 0 & 0 & 1 & 0 & -1 & -1 \\ 0 & 0 & 0 & 4 & 0 & 0 \\ 0 & 0 & 0 & 0 & 4 & 0 \\ 0 & 0 & 0 & 0 & 0 & 4 \end{bmatrix} \begin{bmatrix} L_1^2 \\ L_2^2 \\ L_3^2 \\ L_1L_2 \\ L_2L_3 \\ L_3L_1 \end{bmatrix}. \tag{25}$$

Obviously, the vector of interpolation functions can be expressed in the matrix form as

$$\phi = [G][E]. \tag{26}$$

In contrast, for pressure, the following linear shape function is used:

$$\begin{bmatrix} \psi_1 \\ \psi_2 \\ \psi_3 \end{bmatrix} = \begin{bmatrix} L_1 \\ L_2 \\ L_3 \end{bmatrix}. \tag{27}$$

Here, the vector of linear shape function is symbolized by $[R]$.

The three shape functions L_1, L_2 and L_3 of the cylindrical coordinates are defined as:

$$L_i = \frac{1}{2A_{area}} (a_i + b_i r + c_i z), (\forall i = 1,2,3).$$

Where A_{area} is the area of the element's triangular and a_i, b_i, and c_i are coefficients. Consequentially, by using the theory of area coordinates for triangular elements, the mass matrix can be expressed as:

$$[M] = \int_{\Omega^e} \phi\phi^\dagger d\Omega = \int_{A^e} \int_0^{2\pi} [G][E][E^\dagger][G^\dagger] r d\theta dA = 2\pi \int_{A^e} [G][E][E^\dagger][G^\dagger] r dA,$$

where,

$$r_m = \frac{r_1 + r_2 + r_3}{3}, z_m = \frac{z_1 + z_2 + z_3}{3}.$$

$$[M] = 2\pi r_m [G]\underline{[E][E^\dagger]}[G^\dagger] \int_{A^e} dA = 2\pi r_m A_{area} [G]\underline{[E][E^\dagger]}[G^\dagger]. \tag{28}$$

The integrate by using the exact integral formula of

$$\int_{A^e} L_1^a L_2^b L_3^c dA = 2A_{area} \frac{a!\, b!\, c!}{(a + b + c + 2)!}.$$

Now, we can to find the derivative form of shape functions as follows:

$$\frac{\partial \phi}{\partial r} = [G]\frac{\partial [E]}{\partial r} = [G][B][R],$$

$$\frac{\partial \phi}{\partial \theta} = 0,$$

$$\frac{\partial \phi}{\partial z} = [G]\frac{\partial [E]}{\partial z} = [G][C][R],$$

$$\frac{\partial \psi}{\partial r} = \frac{\partial [R]}{\partial r} = [T],$$

$$\frac{\partial \psi}{\partial z} = \frac{\partial [R]}{\partial z} = [S],$$

where,

$$[B] = \frac{1}{2A_{area}}\begin{bmatrix} 2b_1 & 0 & 0 \\ 0 & 2b_2 & 0 \\ 0 & 0 & 2b_3 \\ b_2 & b_1 & 0 \\ 0 & b_3 & b_2 \\ b_3 & 0 & b_1 \end{bmatrix}, \quad [C] = \frac{1}{2A_{area}}\begin{bmatrix} 2c_1 & 0 & 0 \\ 0 & 2c_2 & 0 \\ 0 & 0 & 2c_3 \\ c_2 & c_1 & 0 \\ 0 & c_3 & c_2 \\ c_3 & 0 & c_1 \end{bmatrix}.$$

$$[T] = \frac{1}{2A_{area}}\begin{bmatrix} b_1 \\ b_2 \\ b_3 \end{bmatrix}, [S] = \frac{1}{2A_{area}}\begin{bmatrix} c_1 \\ c_2 \\ c_3 \end{bmatrix}.$$

Also, the final diffusion matrix formula can be written as:

$$S^{rr} = 4\pi r_m A_{area}[G][B]\underline{[R][R^\dagger]}[B^\dagger][G^\dagger] + \frac{4\pi}{r_m}A_{area}[G]\underline{[E][E^\dagger]}[G^\dagger]$$
$$+2\pi r_m A_{area}[G][C]\underline{[R][R^\dagger]}[C^\dagger][G^\dagger], \quad (29)$$

$$S^{rz} = 2\pi r_m A_{area}[G][B]\underline{[R][R^\dagger]}[C^\dagger][G^\dagger], \quad (30)$$

$$S^{\theta\theta} = 2\pi r_m A_{area}[G][B]\underline{[R][R^\dagger]}[B^\dagger][G^\dagger] - 2\pi A_{area}[G][B]\underline{[R][E^\dagger]}[G^\dagger]$$
$$+\frac{4\pi}{r_m}A_{area}[G]\underline{[E][E^\dagger]}[G^\dagger] - 2\pi A_{area}[G]\underline{[E][R^\dagger]}[B^\dagger][G^\dagger]$$
$$+2\pi r_m A_{area}[G][C]\underline{[R][R^\dagger]}[C^\dagger][G^\dagger], \quad (31)$$

$$S^{\theta z} = (S^{z\theta})^\dagger = S^{r\theta} = (S^{\theta r})^\dagger = 0, \quad (32)$$

$$S^{zr} = 2\pi r_m A_{area}[G][C]\underline{[R][R^\dagger]}[B^\dagger][G^\dagger], \quad (33)$$

$$S^{zz} = 2\pi r_m A_{area}[G][B]\underline{[R][R^\dagger]}[B^\dagger][G^\dagger] + 4\pi r_m A_{area}[G][C]\underline{[R][R^\dagger]}[C^\dagger][G^\dagger]. \quad (34)$$

Moreover, the element of convective matrix is defined as

$$[C(u_r, u_\theta, u_z)] = [C_r(u_r)] + [C_\theta(u_\theta)] + [C_z(u_z)],$$

$$[C_r(u_r)] = 2\pi r_m A_{area}[G]\underline{[E][E^\dagger]}[G^\dagger][u_r]\underline{[R^\dagger]}[B^\dagger][G^\dagger], \quad (35)$$

$$[C_z(u_z)] = 2\pi r_m A_{area}[G]\underline{[E][E^\dagger]}[G^\dagger][u_z]\underline{[R^\dagger]}[C^\dagger][G^\dagger], \quad (36)$$

$$[D_1(u_\theta)] = -2\pi A_{area}[G]\underline{[E][E^\dagger]}[G^\dagger][u_\theta]\underline{[E^\dagger]}[G^\dagger], \quad (37)$$

$$[D_2(u_\theta)] = 2\pi A_{area}[G]\underline{[E][E^\dagger]}[G^\dagger][u_\theta]\underline{[E^\dagger]}[G^\dagger], \quad (38)$$

$$[C_\theta(u_\theta)] = 0.$$

Also, the divergence/pressure gradient matrix is defined as:

$$\ell_r = 2\pi r_m A_{area}\underline{[R][R^\dagger]}[B^\dagger][G^\dagger] + 2\pi A_{area}\underline{[R][E^\dagger]}[G^\dagger], \quad (39)$$

$$\ell_\theta = 0, \ell_z = 2\pi r_m A_{area}\underline{[R][R^\dagger]}[C^\dagger][G^\dagger]. \quad (40)$$

Finally, the pressure stiffness matrix is given by

$$[K] = 2\pi r_m A_{area}\underline{[T][T^\dagger]} + 2\pi r_m A_{area}\underline{[S][S^\dagger]}. \quad (41)$$

4. Problem specifications and boundary conditions

Poiseuille flow through a two-dimensional axisymmetric straight channel was introduced in this study under isothermal conditions. Symmetry of the flow centerline is taken, permitting solutions to be sought over the upper, where the radial velocity at the centerline vanishes. For this purpose, three different triangular finite element meshes are implemented: a cross mesh of (2×4) elements, medium mesh of (5×10) elements, and fine mesh of (10×20) elements with the same length, as shown in Fig.1 (Typical finite element mesh characteristics are included in Table 1).

Boundary conditions (BCs): The setting of BC_s of the present channel problem is laid as follows:

(a) Poiseuille (Ps) flow is specified at the inlet with zero radial velocity .

(b) No-slip BCs were applied to the top and bottom walls of the channels.

(b) Zero radial velocity is applied and zero pressure is applied to the outlet of the channels.

Table 1: Mesh characteristic parameters

Mesh	Total Element	Total Nodes	Boundary Nodes	Pressure Nodes
Cross mesh (M1)	8	25	16	9
Medium mesh (M2)	50	121	40	36
Fine mesh (M3)	200	441	80	121

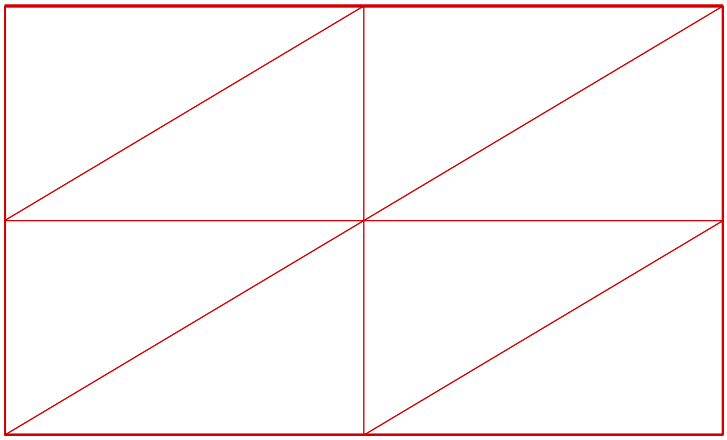

(a) Cross mesh M1: (2×4) elements

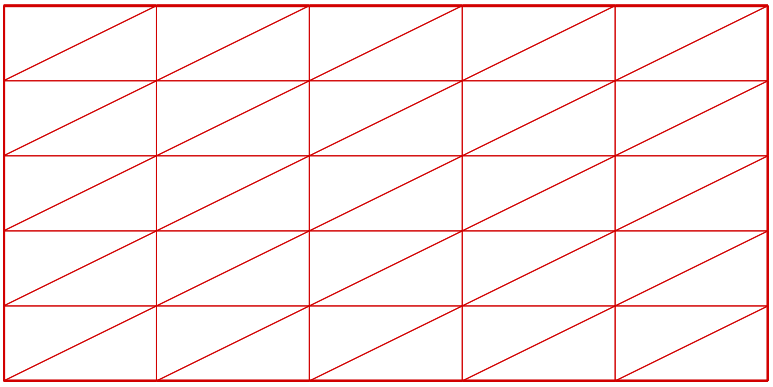

(b) Medium mesh M2: (5×10) elements

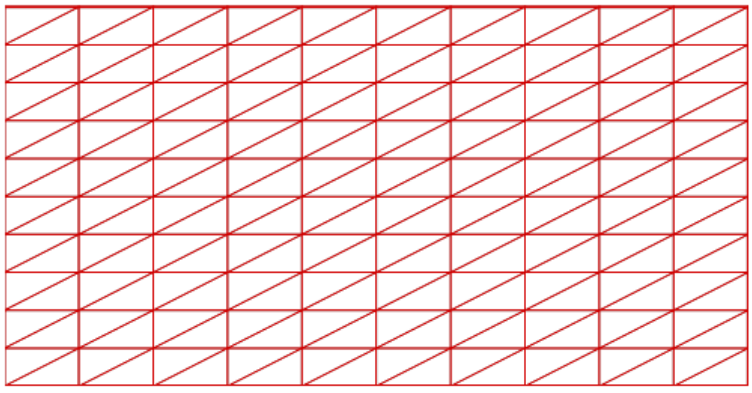

(c) fine mesh M3: (10×20) elements

Figure 1: mesh pattern

5. Numerical results

The numerical results are computed for Newtonian flow through an axisymmetric straight channel by taking a circular cross section of the pipe. In this representation, three different triangular finite element meshes were used to present the numerical analysis results under different mesh convergence levels. The results are shown for $R = 1$, Crank-Nicolson parameter $\theta = 0.5$, tolerance criteria taken here as 10^{-14} and typical Δt is $O(10^{-3})$. The critical of (Re) are evaluated for three meshes and μ varying between 0 and 2. In addition, the results concerned also with the rate of error convergence of the problem components under Re-variation. The exact solution for the problem under consideration with specific conditions has introduced to compare with the numerical results in velocity at the in fully developed flow area.

Exact solution: For fully developed shear axisymmetric fluids through a circular channel, the solution in velocity can be computed analytically under specific conditions. In this case, for the axis of symmetry $r = 0$ and top wall $r = R$, we have the dimensional velocity solution in the form

$$u_z = (u_z)_{max}\left(1 - \frac{r^2}{R^2}\right), \qquad (42)$$

where, R is the radial of the channel and $(u_z)_{max}$ is the maximum velocity in the fully developed flow area, which is defined as [17]

$$(u_z)_{max} = \frac{R^2 \Delta p}{4\mu_s l}, \qquad (43)$$

such that, $\Delta p = p_2 - p_1$, where p_1 and p_2 are the pressures at the outlet and inlet of the pipe, respectively, and l is its length.

In our study, to compare the numerical results with the exact solution for fully developed velocity the simulation was implemented for $R = 1$ with applying same conditions. The profile of the analytical and numerical axial velocities in the fully developed flow (zone $z = 1$) is presented in Figure 2. The numerical result is provided for fine mesh, $Re = 1$ and $\mu = 1$, under imposing axial velocity corresponding to analytical expressions for fully-developed (42), with $(u_z)_{max}$ set to 2. Findings show that, the obtained numerical results are given a perfect

agreement with available analytical solutions, which reflects the sufficiently of the $TS-TG/PC-FEM$ (see Figure 2).

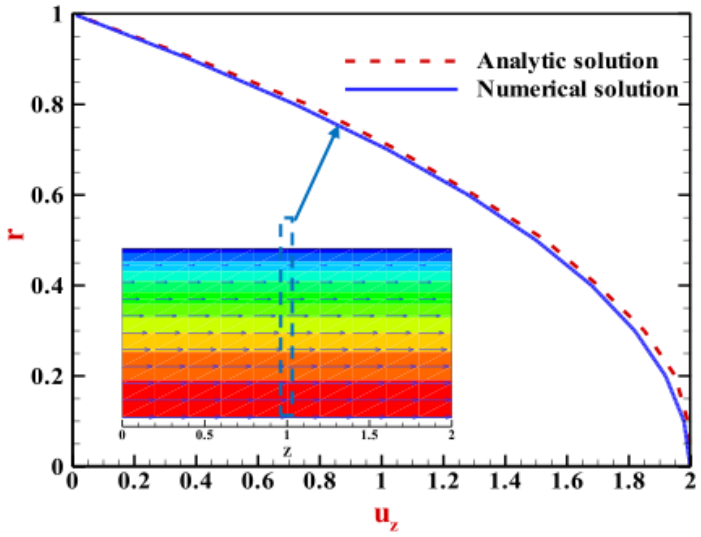

Figure 2: Cross-channel axial velocity profiles: fine mesh, $Re = 1, \mu = 1$

In Figure 3, field plots are presented for the velocity and pressure for the fine mesh. As to be anticipated, a maximum level of velocity is displayed along the center line of the channel (2 units), and then decreases gradually by going to the above. Also, the level of pressure rise at the inlet of the tube reduces whenever closer to the outlet of the tube with a maximum around 16 units.

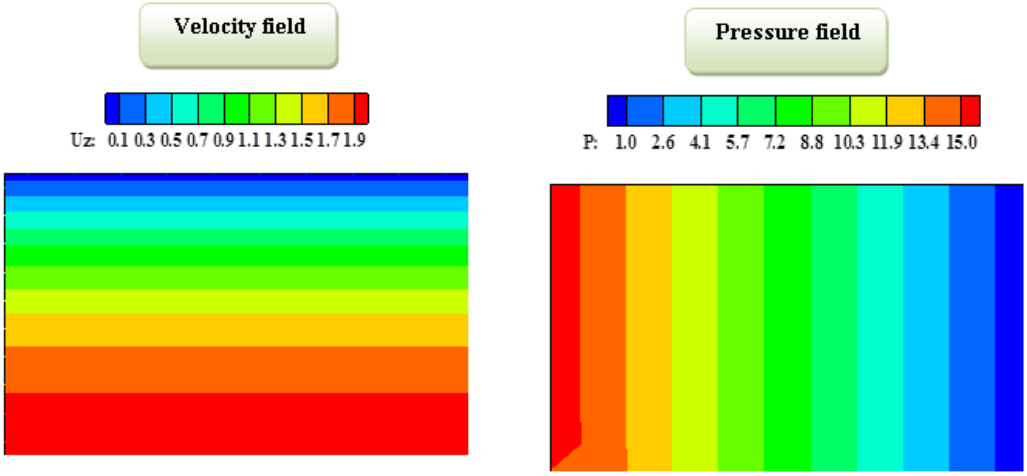

Fig. 3: Velocity and pressure fields: fine mesh, $Re = 1, \mu = 1$

The channel pressure distribution along the axis of symmetry for the cross mesh and fine mesh with fixed $Re = 1$ and $\mu = 1$ is provided in Figure 4a. For the two meshes, a linear decline in pressure occurs throughout the center of the channel, after which the pressure reaches zero at the outlet of the channel. From this data, the pressure level is rise from 8 units with a cross mesh to around 15 units for fine mesh (almost double) at the inlet of the channel, and continuity with the same feature until they arrived to finish point. In addition, the pressure drop is plotted in Figure 4b for the fine mesh with $Re = \{10, 50, 65\}$. The profiles displayed that there is an insignificant effect of Re-variation on the pressure distribution over the channel, in spite of a slight change in the zone of $0 < Z < 0.2$ (as shown in the zoom section). The same situation appeared for cross and medium meshes (not shown).

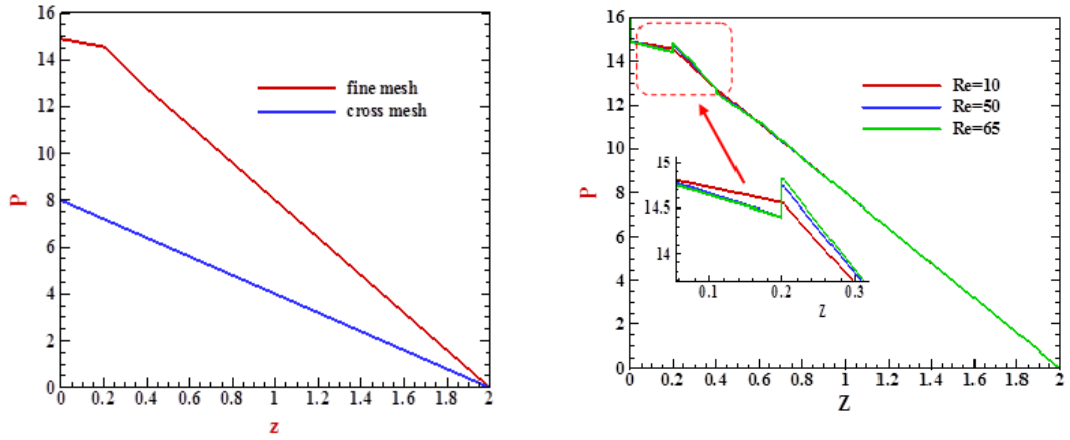

(a) (b)

Fig. 4: Pressure drop profiles on axis of symmetry: (a) cross mesh vs fine mesh, $Re = 1, \mu = 1$ (b) Re-variation, fine mesh and $\mu = 1$

The critical Reynolds number (Re_{cri}) for the three meshes is illustrated in Table 2 under three levels of $(u_z)_{max} = \{1, 1.5, 2\}$,which applies for inlet flow. Here, an explicit comparison in Re_{cri}, where the results show that the critical level was that of $Re_{cri} \sim O(460)$, $Re_{cri} \sim O(240)$ and $Re_{cri} \sim O(65)$ for cross, medium, and fine meshes, respectively. The results reflect the effect of the size of the element on the level of Reynolds number. In addition, the critical Reynolds number (Re_{cri}) for different settings of $(u_z)_{max}$ is given in Table 3. From

the results, one can conclude that the level of Re_{cri} is noticeably affected by the inlet boundary maximum axial velocity, where decreases $(u_z)_{max}$ leads to a larger level of Re_{cri}.

Table 2: Critical Reynolds number (Re_{cri}) for three different meshes with $\mu = 1$.

Mesh	Critical Re (Re_{cri})
Cross mesh (M1)	460
Medium mesh (M2)	240
fine mesh (M3)	65

Table 3: Critical Reynolds number (Re_{cri}) for different level of axial inlet velocities; cross mesh

$(u_z)_{max}$	Critical Re (Re_{cri})
1	460
1.5	300
1.6	285
1.7	160
1.8	240
2	220

To see the influence of $(u_z)_{max}$ that applied at the inlet of the tube on the level of the critical Re, Figure 5a demonstrates critical Re profile as a function of viscosity $0 < \mu < 2$. Here, the critical level of Re is observed to decrease as the viscosity raises such that the maximum of Re_{cri} corresponds to the smallest viscosity, $\mu = 0.001$, which is consistent with the natural of the characteristic non-dimensional equation of Reynolds number ($Re = \frac{\rho U l}{\mu}$). Moreover, one can observe that the level of critical Re is increased as the $(u_z)_{max}$ decreases, which reflect the fact of the effect of boundary inlet velocity on the critical.

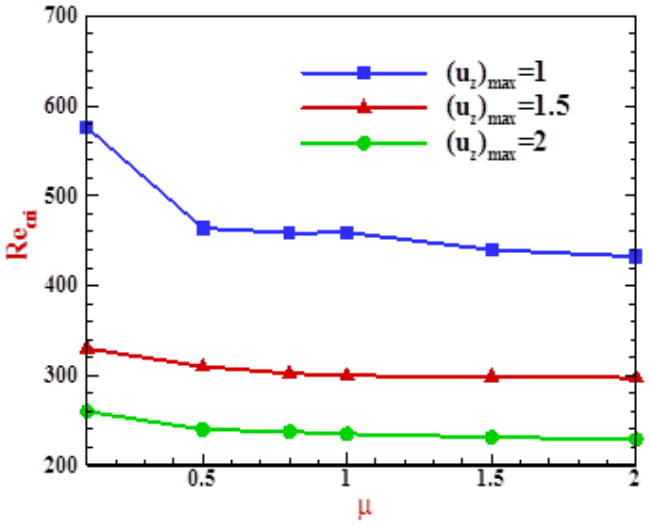

Fig. 5: Critical Reynolds number (Re_{cri}) vs. viscosity.

Figure 6 shows the level of pressure distribution along the axis of symmetry for rising $(u_z)_{max}$. For various $(u_z)_{max}$, a rapid linear decline in pressure happens during the channel, after which the pressure value reaches sharply to zero at the end of the channel. For more illustration of the behaviour of flow, the profiles also provided that the maximum axial velocity at the entry of the channel needs a high level of pressure to achieve a fully developed situation.

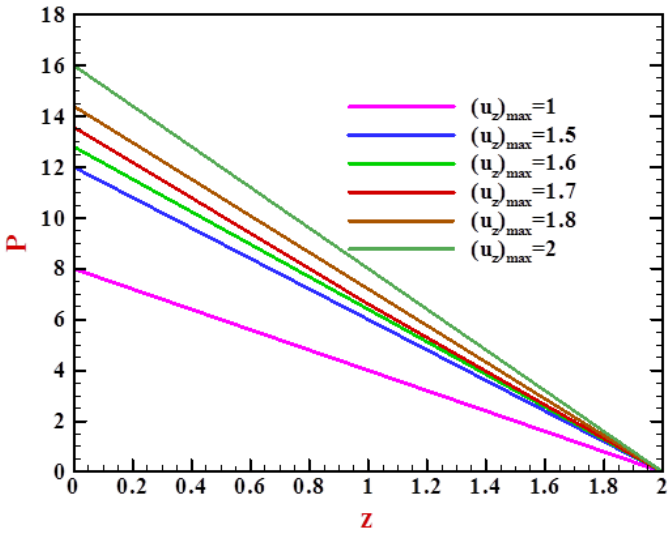

Figure 6: Pressure profile, cross mesh, $(u_z)_{max}$-variation, $\mu = 1, Re = 1$

Geometry characteristic effect: to interrogate the influence of the channel length on the level pressure drop, the simulation was conducted using four different fine triangular finite element meshes, M3, M4, M5, and M6 with height $h = 1$ and various lengths $L = 2, L = 3, L = 4$, and $L = 5$, respectively, as shown in Figure 7.

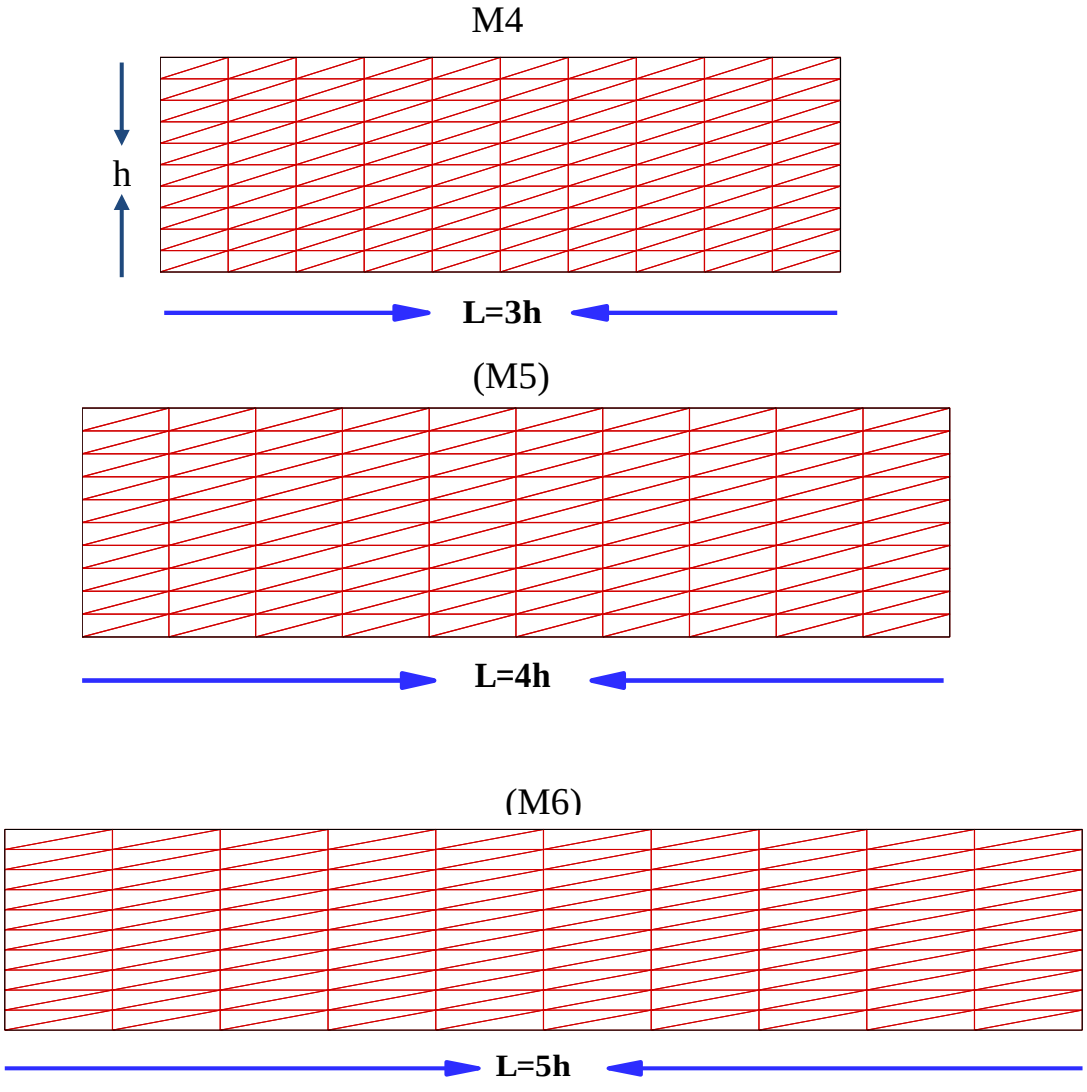

Figure 7: Finite element mesh, (M3) L=2, (M4) L=3, (M5) L=4, (M6) L=5.

Pressure drop: In Figure 8, field plots are presented for pressure with $L = \{3, 4, 5\}$ and fixed $Re = 1$. As to be anticipated, a maximum level of pressure is displayed at the inlet of the channel, and then decreases gradually by going to the cone exit. The fields show that there is a significant effect of the channel length on the level of pressure, and the level of pressure rise as increase L to reach the high level with maximum around 40 units with $L = 5$.

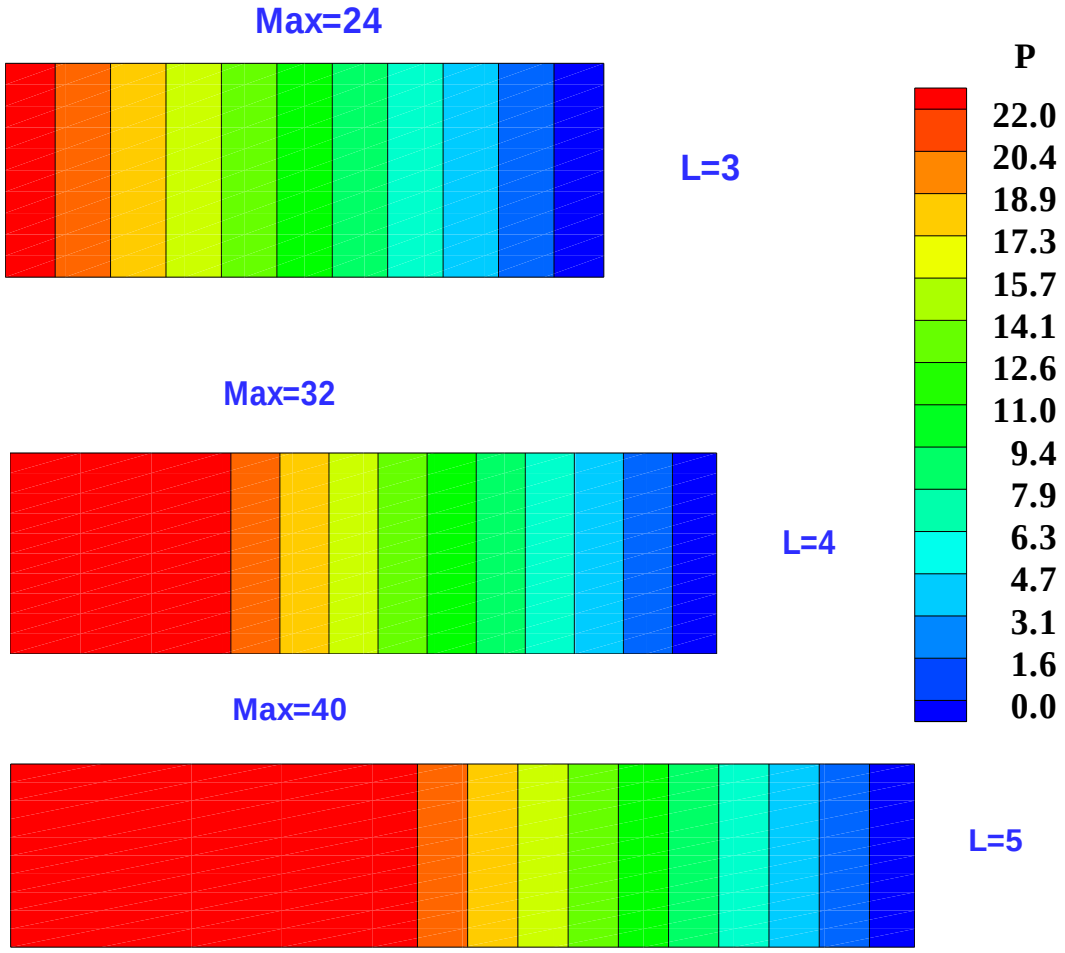

Fig. 8: Pressure fields, L-variation, $Re = 1$.

In addition, pressure drop is plotted in Figure 9 with L variation and $Re = 1$, along the axis of symmetry. The profiles displayed that there is a significant effect of L-variation on the

pressure distribution over the channel. In this context, the level of pressure drop is raised as L increased, reaching a peak of 40 with $L = 5$.

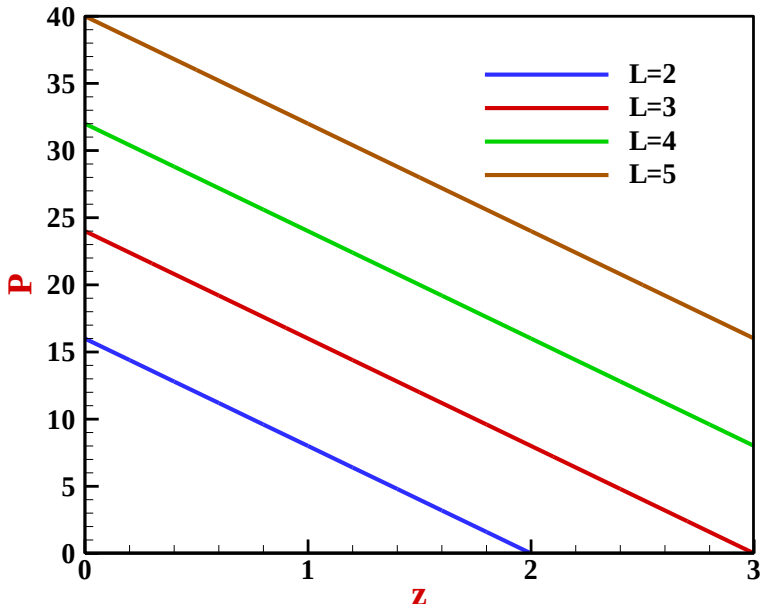

Fig. 9: Pressure drop profiles on the axis of symmetry; L-variation, $Re = 1$

Pressure coefficient (C_p): other finding of our investigation is the pressure coefficient (C_p), which is defined as:

$$C_p = \frac{p_1 - p_0}{\frac{1}{2}\rho \overline{U}^2}. \qquad (44)$$

Where, p_1 is the pressure at the channel inlet, p_0 is the pressure at the channel outlet, ρ is the density, and $\overline{U}$ is the average velocity. Here, the pressure coefficient is studied for different setting of Re and channel length L. Consequently, Figure 10 illustrated the C_p as a function of Re with $L = \{2, 3, 4, 5\}$. The results reveal that, the level of C_p is increased as the length of channel raised as expected, while notable reducing is occurred as Re increases, which is consistent with the results reported by Garrioch and James [18]. Due to the inertial effects dominated, one can observe that at high Re, the C_p curves tend to the lower limit, reaching to around 1 unit.

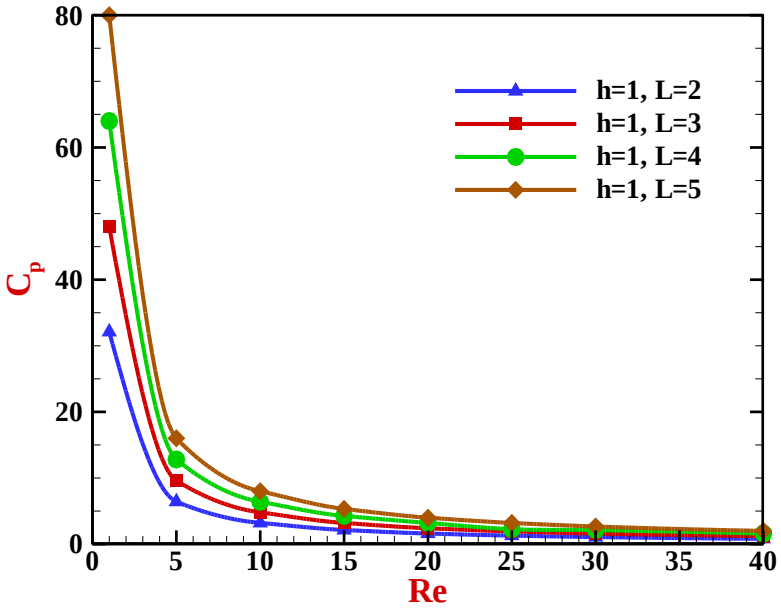

Fig. 10: Pressure drop coefficient for L-variation.

6. Conclusions

In this study, the numerical simulation for laminna incompressible Newtonian fluid is achieved based on is the Taylor-Galerkin pressure correction method in a Cylindrical coordinate system. With the selected set of parameters, we commenced with a Reynolds number (Re) and viscosity (μ). In addition, the influence of the inlet boundary condition on the behavior of axisymmetric incompressible Newtonian flow was studied as well. The exact solution for the problem under consideration with specific conditions was introduced to compare with the numerical results in velocity at the in fully developed flow area. In this matter, an excellent accuracy of the solution appears compared with the exact solution. The critical level of Re number is investigated for three types of meshes, where we found that the maximum level appears with a cross mesh; this reaches around 460. In contrast, the impact of viscosity variation on the critical level of Re number is also studied. In this situation, and as it is anticipated, we found that a high level of Re number has occurred with a low level of viscosity. In addition, the

effect of the boundary maximum axial velocity $(u_z)_{max}$ at the inlet of channel on the level of density and Re number is investigated under μ-variation. In this status, we dedected that there is a significant effect of $(u_z)_{max}$ upon the level of Re number and density, such that was generally found that decreasing $(u_z)_{max}$ increases Re number and density. In the case of Re number, one can see that the maximum Re was around 576 with $(u_z)_{max} = 1$ and $\mu = 0.1$ units, while with the same value of $(u_z)_{max}$ the density level reaches around 865 units with $\mu = 2$ units. Ultimately, the effect of channel length on the pressure drop and coefficient (C_p) is presented as well. In this context, considerable impact is observed for varying of the channel length on the both pressure drop and pressure coefficient.

References

[1] R. B. Bird, R. C. Armstrong, O. Hassager, Dynamics of polymeric liquids, Vol.1: Fluid mechanics. 1987.

[2] P.Townsend and M.F.Webster, An algorithm for the three-dimensional transient simulation of non-Newtonian fluid flows. In: Proc. Int. Conf. Num. Meth. Eng.: Theory and Applications, NUMETA, Nijhoff, Dordrecht, 1987.

[3] A. J. Chorin, Numerical solution of the Navier-Stokes equations, Math. Comput., 22 (1968) 745-762.

[4] P. M. Gresho, R. L. Lee, and R. L. Sani, On the time-dependent solution of the incompressible Navier-Stokes equations in two and three dimensions, In Recent Advances in Numerical Methods in Fluids, Pineridge Press Limited, Swansea, 1980.

[5] J. Donea, S. Giuliani, H. Laval, and L. Quartapelle, Finite element solution of the unsteady Navier-Stokes equations by a fractional step method, Comput. Methods Appl. Mech. Eng., 30 (1982) 53-73.

[6] M. Kawahara and K. Ohmiya, Finite element analysis of density flow using the velocity correction method, Int. J. Num. Meth. Fluids, 5 (1985) 981-993.

[7] A. Al-Muslimawi, Taylor Galerkin Pressure Correction (TGPC) Finite Element Method for Incompressible Newtonian Cable-Coating Flows., Journal of Kufa for Mathematics and Computer, 5 (2018)13-21.

[8] J. Donea, A Taylor–Galerkin method for convective transport problems, Int. J. Num. Meth. Eng. 20 (1984) 101–119.

[9] O. C. Zinenkiewicz, K. Morgan, J. Peraire, M. Vandati, R. Löhner, Finite elements for compressible gas flow and similar systems. In: 7th Int. Conf. Comput. Meth. Appl. Sci. Eng., 1985.

[10] D. M. Hawken, H. R. Tamaddon-Jahromi, P. Townsend, M.F. Webster, *A Taylor Galerkin based algorithm for viscous incompressible flow*, Int. J. Num. Meth. Fluids 10 (1990) 327-351.

[11] M. Aboubacar, H. Matallah, M.F. Webster, Highly elastic solutions for Oldroyd-B and Phan-Thien/Tanner fluids with a finite volume/ element method: planar contraction flows, J. Non-Newton. Fluid Mech. 103 (2002) 65–103.

[12] D. M. Hawken, P. Townsend, and M. F. Webster, *Numerical simulation of viscous flows in channels with a step*, Comput. Fluids 20 (1991) 59-75.

[13] H. T. Jahromi, M. F. Webster, and P. R. Williams, *Excess pressure drop and drag calculations for strain-hardening fluids with mild shear-thinning: Contraction and falling sphere problems*, J. Non-Newton. Fluid Mech., 166 (2011) 939-950.

[14] I. C. Slattery, A.J. Giacomin, F. Ding, Wire coating by drawdown of an extruded annular melt, Int. Polym. Processing 2 (1999) 152-158.

[15] B. K. Jassim, A. Al-Muslimawi, Numerical analysis of Newtonian flows based on artificial compressibility AC method, J. of Al-Qadisiyah for computer science and mathematics, 9 (2017) 115-128.

[16] A. Al-Muslimawi, Numerical analysis of partial differential equations for viscoelastic and free surface flows, PhD thesis, University of Swansea, 2013.

[17] L. D. Landau, and E. M. Lifshitz, Fluid Mechanics. Second Edition. Pergamon, Oxford 1987.

[18] S. H. Garrioch, and D. F. James, A finite-element study of Newtonian and power-law fluids in conical channel flow. J. Fluids Eng., 119 (1997) 341-346.

محاكاة تدفق الأنابيب النيوتونية المحورية باستخدام طريقة تايلر كالركن لتصحيح الضغط للعناصر المحددة

احسان عقيل فاضل[1] علاء حسن المسلماوي [2]

[1] جامعة تالبصرة, كلية التربية للعلوم الصرفة, قسم الرياضيات.

[2] جامعة تالبصرة, كلية العلوم, قسم الرياضيات.

المستخلص

في هذه الدراسة تم استخدام طريقة تايلر كالركن لتصحيح الضغط للعناصر المحددة لمعالجة التدفق النيوتوني غير المضغوط. في هذه الحالة تستخدم معادلات نافير ستوك لوصف حركة السوائل وتتكون هذه المعادلات من معادلة الاستمرارية ومعادلة الزخم المعتمدة على الزمن ولتوضيح الدراسة تم اخذ مثال تطبيقي في نظام الاحداثيات الكروية لتدفق داخل قناة. ان دراسة المستوى الحرج لعدد رينولدز كانت واحدة من النقاط الاساسية في هذه الدراسة كذلك الحال في دراسة تاثير السرعة العظمى التي تسلط في مدخل القناة على مستوى عدد رينولدز حيث وجد ان اعلى مستوى يمكن ان يصل له عدد رينولدز هو 576 عندما $(u_z)_{max} = 1$ ، $\mu = 1$. كذلك تم دراسة تاثير تغير اللزوجة على عدد رينولدز حيث تم مشاهدة نتائج مغايرة لما حصل في حالة تغير السرعة العظمى. تمت تغطية تأثير التصميم الهندسي على مستوى انخفاض الضغط ومعامل الضغط في هذا البحث.